Applied Mathematics and Computation 265 (2015) 681–695

Contents lists available at ScienceDirect

Applied Mathematics and Computation

journal homepage: www.elsevier.com/locate/amc

A Robust and accurate Riemann solver for a compressible two-phase flow model

Sahadeb Kuila [a], T. Raja Sekhar [a], D. Zeidan [b,*]

[a] Department of Mathematics, Indian Institute of Technology Kharagpur, Kharagpur-2, India
[b] School of Basic Sciences and Humanities, German Jordanian University, Amman, Jordan

ARTICLE INFO

Keywords:
Hyperbolic conservative PDEs
Drift-flux model
Riemann problem
Exact solver
Finite volume
Godunov centred methods

ABSTRACT

In this paper we analyze the Riemann problem for the widely used drift-flux two-phase flow model. This analysis introduces the complete information that is attained in the representation of solutions to the Riemann problem. It turns out that the Riemann waves have rarefactions, a contact discontinuity and shocks. Within this respect, an exact Riemann solver is developed to accurately resolve and represent the complete wave structure of the gas-liquid two-phase flows. To verify the solver, a series of test problems selected from the literature are presented including validation against independent numerical simulations where the solution of the Riemann problem is fully numerical. In this framework the governing equations are discretized by finite volume techniques facilitating the application Godunov methods of centred-type. It is shown that both analytical and numerical results demonstrate the broad applicability and robustness of the new exact Riemann solver.

1. Introduction

The subject of multiphase flows has become increasingly important in engineering design and operations such as wellbores, chemical reactors and nuclear industry. Mathematical modelling of two-phase flows within such context depend on the theoretical details of the problem in hand and on the range of approaches and computational resources available for such flows. However, many studies towards two-phase flows have been presented in the literature. These in general include empirical correlations, homogeneous models and mechanistic models [1–3]. In practical situations, mechanistic models are often considered as they are known to provide more details about the physics of each fluid pattern. The mathematical description of such models, however, is not significantly different from those less demanding two-phase flow models. The challenge among these models is always related to the hyperbolicity and conservativity nature of the governing equations [4–6]. Despite the challenges, interest in these models have remained high and the number of research developments has grown steadily. See for example [7–10] and references therein.

One of the simplest mechanistic models is the drift-flux model. The drift-flux model, or approach, results from averaging of the mathematical equations for single-phase flow and consists of a continuity equation for each phase, and a momentum equation for the mixture. The drift-flux model was first proposed by Zuber and Findlay [1] and has been advanced by many researchers for two-phase flow analysis (see, *e.g.* [10–13] and the references therein). This is due to its simplicity, transparency and accuracy in various industrial applications such as thermal-hydraulic analysis codes, wellbores and the reservoir simulators

* Corresponding author. Tel.: 065150593.
E-mail addresses: trajasekhar@maths.iitkgp.ernet.in (T. Raja Sekhar), diazeidan@yahoo/gmail.com, dia.zeidan@gju.edu.jo (D. Zeidan).

http://dx.doi.org/10.1016/j.amc.2015.05.086
0096-3003/

[9,14–18]. Furthermore, the number of publications related to such a model has increased recently and some fundamental and challenging issues still remained unsolved, such as the Riemann problem to the model equations. The drift-flux model takes into account the slip motion between phases by a constitutive relation [1,14]. This relation makes it very challenging and difficult to aim for a closed form, analytical, solutions. Due to the complicated nature of the resulting differential equations, early analytical solutions were based on certain simplifications such as the steady-state homogeneous flow (see for example [14,18–22]). Our objective in this paper, therefore, is to move forward beyond such analysis and explore general properties of the drift-flux model. Furthermore, we present an analytical procedure to solve the drift-flux model of unsteady-state and compressible two-phase flows. The solution is based on the Riemann problem for the model equations. As regard to the Riemann problem, it has achieved a considerable importance in two-phase fluid flow problems and several authors have proposed numerical methods based on solving the Riemann problem solutions. In [23] an exact solver for homogeneous Baer–Nunziato model (see, [24]) was developed on the basis of inverse solution to the Riemann problem. That is, the authors fixed the solution of the Riemann problem and then they look for initial data which are compatible with the assumed wave configuration. The authors in [25] have also developed a solution to the Riemann problem for the Baer–Nunziato model of compressible two-phase flows for given initial data. Another exact solution was also developed in [26] for the Riemann problem for the five equation two-phase non-conservative model of [7]. In [27] a direct, non-linear Riemann solver for two-phase flow in gas-liquid mixture was developed and employed locally within the framework of finite volume upwind Godunov methods.

In this paper we investigate the Riemann problem for a hyperbolic system of partial differential equations governing the known drift-flux model for two-phase flows (see, [28] and the references therein). Unlike single equation methods noted in the conventional ideal gas-dynamics, the present approach is based on the system of two non-linear equations imposing the equality of common velocity and the pressure on the two sides of contact discontinuity. We solve the non-linear algebraic system using Newton–Raphson iterative procedure with a stopping criteria where the relative error is less than 10^{-8}; the initial guess for the intermediate unknown physical quantity is taken to be the average of left and right state. The solution to the Riemann problem provides a building block for a wide class of numerical methods such as Godunov methods [29]. Finally, the exact solution to the Riemann problem is an invaluable test case which is useful in assessing the performance of numerical methods as we shall see in the current paper.

The structure of this paper as follows. In Section 2, we recall the drift-flux model. In Section 3, we discuss the properties of elementary waves, namely, rarefaction waves, shock waves and contact discontinuities of the Riemann problem associated with the model equations. In Section 4 , we give the full details for the construction of Riemann solutions. In Section 5, we describe the numerical method used to validate the developed Riemann solver. A number of test cases conducted during our investigation are presented in Section 6. These test cases are based on the exact solution to the Riemann problem. Finally, conclusions are given in Section 7.

2. Governing equations

The two-phase fluid flow model considered in this paper is based on the Eulerian description of both phases. Such a description has been widely used in the literature where balance equations represent the evolution of mass, momentum and energy for each phase. For isentropic one-dimensional flows these equations are given by two mass and two momentum balance equations for each phase as follows:

$$\frac{\partial}{\partial t}(\rho_g\alpha_g) + \frac{\partial}{\partial x}(\rho_g\alpha_g u_g) = S_1, \tag{1}$$

$$\frac{\partial}{\partial t}(\rho_l\alpha_l) + \frac{\partial}{\partial x}(\rho_l\alpha_l u_l) = S_2, \tag{2}$$

$$\frac{\partial}{\partial t}(\rho_g\alpha_g u_g) + \frac{\partial}{\partial x}\left(\rho_g\alpha_g u_g^2\right) + \frac{\partial}{\partial x}(\alpha_g p_g) = S_3, \tag{3}$$

$$\frac{\partial}{\partial t}(\rho_l\alpha_l u_l) + \frac{\partial}{\partial x}\left(\rho_l\alpha_l u_l^2\right) + \frac{\partial}{\partial x}(\alpha_l p_l) = S_4. \tag{4}$$

Index g in the above system is referred to the gas and l to the liquid phase; x is the space coordinate and t is the time; ρ_j, u_j, p_j and α_j are the density, velocity, pressure and volume fraction of phase j $(j = g, l)$, respectively. The volume fractions are subject to the constraint

$$\alpha_g + \alpha_l = 1. \tag{5}$$

The source terms on the right hand side of Eqs. (1)–(4) depend on the modeled two-phase flow pattern. They consists of constitutive relations for the interface transfers of interest. For the purposes of this paper, we have neglected these source terms and thus it is unnecessary to carry them along in the current theoretical investigation. The above system is closed with the equation of state (EOS) for each phase. In particular, isentropic laws are considered in the following form

$$p_g = p_g(\rho_g) \quad \text{and} \quad p_l = p_l(\rho_l). \tag{6}$$

Thus, the equation of state for a pure liquid and an ideal gas is written as follows

$$p_g = p_g(\rho_g) = K_g \rho_g^{\gamma_g} \quad \text{and} \quad p_l = p_l(\rho_l) = K_l \rho_l^{\gamma_l}, \tag{7}$$

where K_g, K_l, γ_g and γ_l are constants to be specified.

System (1)–(4) is the simplest physical two-fluid model proposed in the literature. As one can note that its mathematical form is not written in a conservative or divergence form. This leads to important mathematical problems related to the character of solutions, and to numerical and theoretical issues related to the problem of calculating solutions of the current model equations. To avoid such difficulties it is necessary to rewrite the model equations in a suitable form such that these non-conservative terms do not appear anymore. This is achieved by adding Eqs. (3) and (4) giving the following mixture momentum

$$\frac{\partial}{\partial t}(\alpha_g \rho_g u_g + \alpha_l \rho_l u_l) + \frac{\partial}{\partial x}\left(\alpha_g \rho_g u_g^2 + \alpha_l \rho_l u_l^2\right) + \frac{\partial}{\partial x}(\alpha_g p_g + \alpha_l p_l) = 0. \tag{8}$$

This approach has the advantage that it provides a set of equations in a straight forward and elegant way to investigate the model equations mathematical structure. It is worth to note that a common assumption for the pressures appearing in (8) is taken into account as

$$p = p_g = p_l, \tag{9}$$

which is a widely used assumption [4,5]. With such formulation in (8), additional relation is required to determine the velocity of each phase separately. This relation is known as the hydrodynamic closure law that takes the following general form [1,2]

$$u_g - u_l = \Phi(p, \alpha_g, u_g), \tag{10}$$

which is also known as the slip relation. To perform mathematical analysis for the Riemann problem of the current drift-flux model then, certain simplifying assumptions need to be made, leading to more simplified governing equations. More specifically, a common assumption within this context of drift-flux modeling is due to the no-slip condition [1], that is, $\Phi = 0$. For the purposes of this paper, therefore, the phase velocities are assumed to be in equilibrium

$$u = u_g = u_l. \tag{11}$$

Eqs. (1), (2) and (8) form a first-order, hyperbolic, non-linear conservative system of partial differential equations for gas-liquid two-phase flow that is known as the drift-flux model as mentioned previously. In the next section we perform the necessary analysis for the development of our exact solver that is based on the Riemann problem.

3. The Riemann solver

3.1. The Riemann problem and system eigenstructure analysis

The model Eqs. (1), (2) and (8) with $S_{1\ldots4} = 0$ can be written in the following conservative form with

$$\frac{\partial U}{\partial t} + \frac{\partial F(U)}{\partial x} = 0, \quad x \in \mathbb{R} \quad \text{and} \quad t \in \mathbb{R}^+, \tag{12}$$

with

$$U = \begin{pmatrix} \rho_l \alpha_l \\ \rho_g \alpha_g \\ \rho_g \alpha_g u_g + \rho_l \alpha_l u_l \end{pmatrix}, \tag{13}$$

and

$$\mathbb{F}(U) = \begin{pmatrix} \rho_l \alpha_l u_l \\ \rho_g \alpha_g u_g \\ \rho_g \alpha_g u_g^2 + \rho_l \alpha_l u_l^2 + \alpha_g p_g + \alpha_l p_l \end{pmatrix}, \tag{14}$$

are the conservative variables and fluxes, respectively.

To further establish the necessary mathematical framework for the current model equations for the development of a robust and accurate exact Riemann solver, we write system (12) in the following alternative form of primitive variables

$$V = [\rho_1, \rho_2, u]^T, \tag{15}$$

where $\rho_1 = \rho_l \alpha_l$ and $\rho_2 = \rho_g \alpha_g$.

As a result, system (12) along with the equation of state $p = k_1 \rho_1^{\gamma_1} + k_2 \rho_2^{\gamma_2}$ and assumption (11) can be written in quasi-linear form as

$$\frac{\partial V}{\partial t} + M(V) \frac{\partial V}{\partial x} = 0, \tag{16}$$

and the Jacobian matrix is given by

$$\begin{pmatrix} u & 0 & \rho_1 \\ 0 & u & \rho_2 \\ \dfrac{\gamma_1 p_1 \rho_1^{-1}}{\rho_1+\rho_2} & \dfrac{\gamma_2 p_2 \rho_2^{-1}}{\rho_2+\rho_2} & u \end{pmatrix}, \tag{17}$$

where $p_1 = k_1\rho_1^{\gamma_1}$ and $p_2 = k_2\rho_2^{\gamma_2}$.

Then one can observe that the characteristic equation has the three real roots

$$\lambda_1 = u - w, \quad \lambda_2 = u \quad \text{and} \quad \lambda_3 = u + w, \tag{18}$$

with

$$w = \sqrt{\frac{\gamma_1 p_1 + \gamma_2 p_2}{\rho_1 + \rho_2}}. \tag{19}$$

The eigenvalues in (18) indicates that system (12) is strictly hyperbolic with the following interpretation as wave speeds

$$\lambda_1(V) < \lambda_2(V) < \lambda_3(V) \quad \forall V. \tag{20}$$

Also, one can note that the characteristics λ_1 and λ_3 coincide with phase pressures and λ_2 corresponds to the flow velocity. Further, the corresponding right eigenvectors are

$$r^{(1)} = \begin{pmatrix} \rho_1 \\ \rho_2 \\ -w \end{pmatrix}, \quad r^{(2)} = \begin{pmatrix} \gamma_2 \dfrac{p_2}{\rho_2} \\ -\gamma_1 \dfrac{p_1}{\rho_1} \\ 0 \end{pmatrix} \quad \text{and} \quad r^{(3)} = \begin{pmatrix} \rho_1 \\ \rho_2 \\ w \end{pmatrix}. \tag{21}$$

From (18) and (21) it is easy to see that the characteristic fields λ_1 and λ_3 are genuinely nonlinear and the characteristic field λ_2 is linearly degenerate. Accordingly, this form the basic structure of the solution of the Riemann problem as a set of elementary waves. The Riemann problem for the current model, therefore, is formulated as a special initial value problem given by (12) for a gas-liquid two-phase flow with discontinuous initial data as

$$U(x,0) = \begin{cases} U^l, & \text{if } x < 0, \\ U^r, & \text{if } x > 0, \end{cases} \tag{22}$$

where U^l and U^r represent the values of the gas and liquid properties on the left and on the right from an interface between the two states at $x = 0$ that exists only at initial time.

3.2. Elementary wave structure of the Riemann problem solution

The elementary wave solutions of the system (12) consists of contact discontinuities, shocks and rarefaction waves.

3.2.1. Shock waves

Let U^l and U denote the left and the right states for either a rarefaction wave or contact discontinuity or shock wave. For a shock wave, the two constant states U^l and U are connected through a single-jump discontinuity in a genuinely nonlinear characteristic field and satisfy the Rankine–Hugoniot (R-H) jump condition:

$$F(U) - F(U^l) = s(U - U^l), \tag{23}$$

where s is the shock speed.

The jump conditions (23) read

$$\rho_1 u - \rho_1^l u^l = s\left(\rho_1 - \rho_1^l\right), \tag{24}$$

$$\rho_2 u - \rho_2^l u^l = s(\rho_2 - \rho_2^l), \tag{25}$$

$$((\rho_1+\rho_2)u^2 + p) - \left(\left(\rho_1^l + \rho_2^l\right)(u^l)^2 + p^l\right) = s\left((\rho_1+\rho_2)u - \left(\rho_1^l + \rho_2^l\right)u^l\right), \tag{26}$$

which on introducing the variable $\tilde{u} = u - s$ become

$$\rho_1 \tilde{u} = \rho_1^l \tilde{u}^l, \tag{27}$$

$$\rho_2 \tilde{u} = \rho_2^l \tilde{u}^l, \tag{28}$$

$$(\rho_1+\rho_2)\tilde{u}^2 + p = \left(\rho_1^l + \rho_2^l\right)(\tilde{u}^l)^2 + p^l. \tag{29}$$

We are going to show that the shocks satisfy the Lax stability conditions.

Theorem 3.1. *Across 1−shock (respectively, 3−shock), $\rho_1^l < \rho_1, \rho_2^l < \rho_2$ and $u^l > u$ (respectively, $\rho_1^l > \rho_1, \rho_2^l > \rho_2$ and $u^l > u$) if, and only if, the Lax conditions hold, i.e.,*

$$\lambda_{i-1}(U^l) < s_i < \lambda_i(U^l), \quad \lambda_i(U) < s_i < \lambda_{i+1}(U). \quad i = 1, 3. \tag{30}$$

Proof. Let us assume that for 1-shock, $\rho_1^l < \rho_1, \rho_2^l < \rho_2$ and $u^l > u$. We show that the Lax conditions hold for $i = 1$. Using (27) and (28) we have $\rho_2 = (\frac{\rho_2^l}{\rho_1^l})\rho_1$, so ρ_2 is a function of ρ_1. Since $p' > 0$ and $p'' > 0$, by Lagrange's mean value theorem, there exists a $\xi \in (\rho_1^l, \rho_1)$ such that $p'(\xi) = (p - p^l)/(\rho_1 - \rho_1^l)$. Furthermore, since $p'' > 0$, we have $p'(\xi) > (p^l)'$. Therefore

$$(w^l)^2 < \left(\frac{p - p^l}{\rho_1^l + \rho_2^l}\right)\left(\frac{\rho_1^l}{\rho_1 - \rho_1^l}\right), \tag{31}$$

this implies

$$-\frac{\rho_1}{\rho_1 - \rho_1^l}\sqrt{\left(\frac{p - p^l}{\rho_1^l + \rho_2^l}\right)\left(1 - \frac{\rho_1^l}{\rho_1}\right)} < -w^l. \tag{32}$$

In view of (24)–(26), the above inequality yields $\rho_1(u - u^l)/(\rho_1 - \rho_1^l) < -w^l$, and hence $s_1 < \lambda_1(V_l) = u^l - w^l$.

Next, since $p'' > 0$ and $\rho_1^l < \rho_1$ for one-shock wave, we have $p'(\eta) = (p - p^l)/(\rho_1 - \rho_1^l) < p'$ for some $\eta \in (\rho_1^l, \rho_1)$. Therefore

$$w^2 > \left(\frac{p - p^l}{\rho_1^l + \rho_2^l}\right)\left(\frac{\rho_1}{\rho_1 + \rho_2}\right), \tag{33}$$

which leads to

$$-w < -\frac{\rho_1^l}{\rho_1 - \rho_1^l}\sqrt{\left(\frac{p - p^l}{\rho_1^l + \rho_2^l}\right)\left(1 - \frac{\rho_1^l}{\rho_1}\right)}. \tag{34}$$

Also, from (24)–(26) imply that $u - w < (\rho_1 u - \rho_1^l u^l)/(\rho_1 - \rho_1^l) = s_1$, and hence $\lambda_1(V) < s_1$.

Lastly, we show that $s_1 < \lambda_2(V) = u$. On the contrary, let us assume that $s_1 \geq u$. For this, we exploit (24), and then it follows that $\rho_1(u - u^l) \geq 0$, which is a contradiction as the left-hand side of the inequality is negative. Hence, one-shock waves satisfy the Lax conditions: the proof for the three-shock waves follows similar lines.

Conversely, we assume that for 1-shock the Lax conditions holds. It follows from (30) that for 1-shock waves, we have $s_1 < u^l - w^l$, where s_1 is the speed of the one-shock wave, which implies that $w^l < \tilde{u}^l$ and $u - w < s_1 < u$, and hence $0 < \tilde{u} < w$. Thus, $w^l < \tilde{u}^l$ and $0 < \tilde{u} < w$ for one-shock waves. Since $\tilde{u} > 0$ and $\tilde{u}^l > 0$, the gas speed on both sides of the shock is greater than the shock speed, so particles cross the shock from the left to the right for one-shock waves. In the case of three-shock waves, the shock inequalities give $-w^l < \tilde{u}^l < 0$ and $\tilde{u} < -w < 0$, which imply that the shock speed is greater than the gas speed on both sides of the shock, and so the particles cross three shocks from the right to the left.

For both the shock families, $\tilde{u}^l$ and $\tilde{u}$ are non-zero so that $L = \rho\tilde{u} = \rho^l\tilde{u}^l \neq 0$. Thus, for one-shock waves, we have $(\tilde{u}^l)^2 > (w^l)^2, w^2 > \tilde{u}^2$ and using (29), we obtain

$$(\rho_1 + \rho_2)w^2 + p > \left(\rho_1^l + \rho_2^l\right)(w^l)^2 + p^l, \tag{35}$$

that is

$$k_1(1 + \gamma_1)\rho_1^{\gamma_1} + k_2(1 + \gamma_2)\rho_2^{\gamma_2} > k_1(1 + \gamma_1)\left(\rho_1^l\right)^{\gamma_1} + k_2(1 + \gamma_2)\left(\rho_2^l\right)^{\gamma_2}, \tag{36}$$

which implies that $\rho_1^l < \rho_1, \rho_2^l < \rho_2$ and so $u^l > u$. In similar way, for three-shock waves, we can prove that $\rho_1^l > \rho_1, \rho_2^l > \rho_2$ and $u^l > u$. Therefore, both the shock waves are compressive. □

For 1-shock waves, using (27)–(28), we obtain ρ_2 and u in terms of ρ_1^l, ρ_2^l, u^l and ρ_1. From (27)–(28), we know

$$\rho_2 = \left(\frac{\rho_2^l}{\rho_1^l}\right)\rho_1. \tag{37}$$

Now from (29), we have

$$(\tilde{u}^l)^2 = \frac{(p^l - p)\rho_1^2}{(\rho_1 + \rho_2)\left(\rho_1^l\right)^2 - \left(\rho_1^l + \rho_2^l\right)\rho_1^2}. \tag{38}$$

Since for one-shock waves, $s_1 - u^l < 0$; from (38), we obtain

$$s_1 = u^l - \sqrt{\frac{(p^l - p)\rho_1^2}{(\rho_1 + \rho_2)\left(\rho_1^l\right)^2 - \left(\rho_1^l + \rho_2^l\right)\rho_1^2}}, \tag{39}$$

and from (24), imply that

$$u = \frac{\rho_1^l u^l}{\rho_1} + \left(\frac{\rho_1 - \rho_1^l}{\rho_1}\right) s_1. \tag{40}$$

Let U and U^r denote the left and the right states for either a three-shock or a three-rarefaction wave. For the three-shock wave, we obtain, in a completely similar manner, all the solutions to (12), are

$$\rho_2 = \left(\frac{\rho_2^r}{\rho_1^r}\right)\rho_1, \tag{41}$$

$$s_3 = u^r + \sqrt{\frac{(p^r - p)\rho_1^2}{(\rho_1 + \rho_2)\left(\rho_1^r\right)^2 - \left(\rho_1^r + \rho_2^r\right)\rho_1^2}}, \tag{42}$$

$$u = \frac{\rho_1^r u^r}{\rho_1} + \left(\frac{\rho_1 - \rho_1^r}{\rho_1}\right) s_3, \tag{43}$$

where s_3 is the speed of the three-shock wave.

3.3. Rarefaction waves

The Riemann invariants $(\mathbf{\Gamma}_1^i, \mathbf{\Gamma}_2^i)$, $i = 1, 2, 3$, along the characteristic fields are given by

$$\mathbf{\Gamma}_1^1 = \frac{\rho_1}{\rho_2}, \qquad \mathbf{\Gamma}_2^1 = u + \int^{\rho_1} \frac{w(\theta)}{\theta} d\theta,$$
$$\mathbf{\Gamma}_1^2 = p, \qquad \mathbf{\Gamma}_2^2 = u,$$
$$\mathbf{\Gamma}_1^3 = \frac{\rho_1}{\rho_2}, \qquad \mathbf{\Gamma}_2^3 = u - \int^{\rho_1} \frac{w(\theta)}{\theta} d\theta.$$

For a rarefaction wave, the two constant states U^l and U are connected through a smooth transition in a i-th genuinely nonlinear characteristic field and the Riemann invariants are constant across the wave. So for one-rarefaction wave,

$$\frac{\rho_1}{\rho_2} = \frac{\rho_1^l}{\rho_2^l}, \quad u + \int^{\rho_1} \frac{w(\theta)}{\theta} d\theta = u^l + \int^{\rho_1^l} \frac{w(\theta)}{\theta} d\theta, \tag{44}$$

which implies

$$\rho_2 = \left(\frac{\rho_2^l}{\rho_1^l}\right)\rho_1, \tag{45}$$

$$u = u^l + \int_{\rho_1}^{\rho_1^l} \frac{w(\theta)}{\theta} d\theta. \tag{46}$$

Similarly, for three rarefaction waves, we have

$$\rho_2 = \left(\frac{\rho_2^r}{\rho_1^r}\right)\rho_1, \tag{47}$$

$$u = u^r - \int_{\rho_1}^{\rho_1^r} \frac{w(\theta)}{\theta} d\theta. \tag{48}$$

Theorem 3.2. *Across 1-rarefaction waves (respectively, 3-rarefaction waves), $\rho_1 < \rho_1^l, \rho_2 < \rho_2^l$ and $u > u^l$ (respectively, $\rho_1 > \rho_1^l, \rho_2 > \rho_2^l$, and $u > u^l$) if and only if, the characteristic speed increases from left hand to right hand state, i.e.,*

$$\lambda_i(V^l) < \lambda_i(V), \quad i = 1, 3. \tag{49}$$

Proof. Let the characteristic speed increases from left hand to right hand state. Therefore from the inequality (49) implies that

$$w - w^l < u - u^l, \tag{50}$$

which by virtue of $(44)_2$ becomes

$$w + \int^{\rho_1} \frac{w(\theta)}{\theta} d\theta < w^l + \int^{\rho_1^l} \frac{w(\theta)}{\theta} d\theta,$$

which implies $\rho_1^l > \rho_1$ and $u^l < u$. From $(31)_1$ using $\rho_1^l > \rho_1$ we have $\rho_2^l > \rho_2$. Similarly, three-rarefaction waves, we can prove that $\rho_1 > \rho_1^l, \rho_2 > \rho_2^l$ and $u > u^l$.

Conversely, for one-rarefaction wave, we assume that $\rho_1^l > \rho_1, \rho_2 > \rho_2^l$ and $u^l < u$. Then we have to prove that the characteristic speed increases from the left to the right, that is, $\lambda_1(V^l) \le \lambda_1(V)$. Using (45), we have $dw/d\rho_1 > 0$, w is an increasing function of ρ_1; this implies that for one-rarefaction waves, $w(\rho_1) \le w(\rho_l^l)$ or equivalently $-w^l \le -w$. From $u^l \le u$ and $-w^l \le -w$ imply that $\lambda_1(V^l) \le \lambda_1(V)$. In similar way, we can prove this for the three-rarefaction waves. □

Theorem 3.3. *The 1-rarefaction curve is convex and monotonic decreasing while 3-rarefaction curve is concave and monotonic increasing.*

Proof. The 1-rarefaction wave is

$$u = \quad u^l + \int_{\rho_1}^{\rho_1^l} \frac{w(\theta)}{\theta} d\theta, \quad \text{if } \rho_1 \le \rho_1^l,$$

which on differentiation with respect to ρ_1, yields
$\frac{du}{d\rho_1} = -\frac{w}{\rho_1} < 0$, and subsequently,

$$\frac{d^2u}{d\rho_1^2} = \frac{w}{\rho_1^2} - \frac{w'}{\rho_1}. \tag{51}$$

Using $p = k_1\rho_1^{\gamma_1} + k_2\rho_2^{\gamma_2}$ and from (45), Eq. (51) yields $\frac{d^2u}{d\rho_1^2} > 0$ and, therefore, u is convex and monotonic decreasing with respect to ρ_1 for 1-rarefaction waves. In a similar way, we can prove that for 2-rarefaction waves. □

3.4. Contact discontinuities

For contact discontinuities, the two constant states U^l and U are connected through a single-jump discontinuity with speed s_2 in the second characteristic field, which is linearly degenerate, and the following conditions hold: (i) the R-H jump conditions

$$F(U) - F(U^l) = s_2(U - U^l), \tag{52}$$

and (ii) the parallel characteristic conditions

$$\lambda_2(U^l) = \lambda_2(U) = s_2. \tag{53}$$

From (53), we get $u = u^l$, and using (53) in (26), we obtain

$$p = p^l, \tag{54}$$

so u and p are constant across the contact discontinuity.

4. Solution strategy

The exact solution of the Riemann problem (12) and (22) has three waves, which are associated with the eigenvalues $\lambda_1 = u - w, \lambda_2 = u$ and $\lambda_3 = u + w$. The three waves separate four constant states, which from the left to the right are V^l, V^-, V^+ and V^r. The middle wave is always a contact discontinuity, while the left and right waves are either shocks or rarefaction waves. Therefore, there are four possible wave patterns depending on the choice of nonlinear waves on the left and right. The common velocity is constant between the left and the right waves, that is, $u^- = u^+$, while the jump of densities of phase 1 and phase 2 across the middle wave is nonzero. Here, we present a solution procedure which makes use of the constancy of common velocity and the pressure p between the left and the right nonlinear waves to derive a system of two algebraic nonlinear equations for ρ_1^- and ρ_1^+. In summary, the main physical quantities to be determined are $s_1, s_3, \rho_1^-, \rho_1^+, \rho_2^-, \rho_2^+$ and u^-.

4.1. Physical quantities across the left shock wave

Substituting the value of s_1 from (39) in (40) and performing some algebraic operations, we get

$$u = u^l - (\rho_1 - \rho_1^l)\sqrt{\frac{(p - p^l)}{\left(\rho_1^l + \rho_2^l\right)\rho_1^2 - (\rho_1 + \rho_2)\left(\rho_1^l\right)^2}}, \tag{55}$$

which in view of (37) yields

$$u = u^l - \sqrt{\frac{\left(\rho_1 - \rho_1^l\right)}{\left(\rho_1^l + \rho_2^l\right)\rho_1}\left(k_1\rho_1^{\gamma_1} + k_2\left(\frac{\rho_2^l}{\rho_1^l}\right)^{\gamma_2}\rho_1^{\gamma_2} - p^l\right)}, \tag{56}$$

$$u^- = u^l - f_l(\rho_1^-, V^l), \tag{57}$$

with

$$f_l(\rho_1^-, V^l) = \sqrt{A_1(\rho_1^-)^{\gamma_1} + A_2(\rho_1^-)^{\gamma_1-1} + A_3(\rho_1^-)^{\gamma_2} + A_4(\rho_1^-)^{\gamma_2-1} + \frac{A_5}{\rho_1^-} + A_6},$$

where

$$A_1 = \frac{k_1}{\rho_1^l + \rho_2^l}, A_2 = -\frac{k_1\rho_1^l}{\rho_1^l + \rho_2^l}, A_3 = \frac{k_2\left(\rho_2^l\right)^{\gamma_2}}{\left(\rho_1^l\right)^{\gamma_2}\left(\rho_1^l + \rho_2^l\right)}, A_4 = -\rho_1^l A_3, A_5 = \frac{p^l\rho_1^l}{\rho_1^l + \rho_2^l}, A_6 = \frac{p^l}{\rho_1^l + \rho_2^l}.$$

Now, we derive an expression for p, which in terms of ρ_1^l, ρ_1^- and ρ_2^l can be expressed as

$$p^- = g_l = k_1(\rho_1^-)^{\gamma_1} + k_2\left(\frac{\rho_2^l}{\rho_1^l}\right)^{\gamma_2}(\rho_1^-)^{\gamma_2} = k_1(\rho_1^-)^{\gamma_1} + B_1(\rho_1^-)^{\gamma_2}, \tag{58}$$

with $B_1 = k_2\left(\frac{\rho_2^l}{\rho_1^l}\right)^{\gamma_2}$.

4.2. Physical quantities across the left rarefaction wave

Since $\mathbf{\Gamma}_2^1$ is constant in the one-rarefaction wave region, we have

$$u + \int^{\rho_1} \frac{w(\theta)}{\theta}d\theta = u^l + \int^{\rho_1^l} \frac{w(\theta)}{\theta}d\theta,$$

$$u^- = u^l - f_l(\rho_1^-, V^l), \tag{59}$$

where

$$f_l(\rho_1^-, V^l) = \int_{\rho_1^l}^{\rho_1^-} \frac{w(\theta)}{\theta}d\theta,$$

which leads to

$$\rho_2 = \left(\frac{\rho_2^l}{\rho_1^l}\right)\rho_1. \tag{60}$$

Now, using (60), we obtain for the rarefaction wave an expression of the sum of densities of both the phases as

$$p^- = g_l = k_1(\rho_1^-)^{\gamma_1} + k_2\left(\frac{\rho_2^l}{\rho_1^l}\right)^{\gamma_2}(\rho_1^-)^{\gamma_2} = k_1(\rho_1^-)^{\gamma_1} + B_1(\rho_1^-)^{\gamma_2}. \tag{61}$$

4.3. Physical quantities across the right shock wave

Substituting the value of s_3 from (42) in (43) and performing some algebraic operations, we get

$$u = u^r + (\rho_1 - \rho_1^r)\sqrt{\frac{(p - p^r)}{(\rho_1^r + \rho_2^r)\rho_1^2 - (\rho_1 + \rho_2)(\rho_1^r)^2}}, \tag{62}$$

which in view of (41) yields

$$u = u^r + \sqrt{\frac{\left(\rho_1 - \rho_1^r\right)}{\left(\rho_1^r + \rho_2^r\right)\rho_1}\left(k_1\rho_1^{\gamma_1} + k_2\left(\frac{\rho_2^r}{\rho_1^r}\right)^{\gamma_2}\rho_1^{\gamma_2} - p^r\right)}, \tag{63}$$

and

$$u^+ = u^r + f_r(\rho_1^+, V^r), \tag{64}$$

with

$$f_r(\rho_1^+, V^r) = \sqrt{C_1(\rho_1^+)^{\gamma_1} + C_2(\rho_1^+)^{\gamma_1-1} + C_3(\rho_1^+)^{\gamma_2} + C_4(\rho_1^+)^{\gamma_2-1} + \frac{C_5}{\rho_1^+} + C_6},$$

where

$$C_1 = \frac{k_1}{\rho_1^r + \rho_2^r}, C_2 = -\frac{k_1\rho_1^r}{\rho_1^r + \rho_2^r}, C_3 = \frac{k_2(\rho_2^r)^{\gamma_2}}{(\rho_1^r)^{\gamma_2}(\rho_1^r + \rho_2^r)}, C_4 = -\rho_1^r C_3, C_5 = \frac{p^r\rho_1^r}{\rho_1^r + \rho_2^r}, C_6 = -\frac{p^r}{\rho_1^r + \rho_2^r}.$$

Now, we derive an expression for p, which in terms of ρ_1^r, ρ_1^+ and ρ_2^r can be expressed as

$$p^+ = g_r = k_1(\rho_1^+)^{\gamma_1} + k_2\left(\frac{\rho_2^r}{\rho_1^r}\right)^{\gamma_2}(\rho_1^+)^{\gamma_2} = k_1(\rho_1^+)^{\gamma_1} + B_2(\rho_1^+)^{\gamma_2}, \tag{65}$$

where $B_2 = k_2\left(\frac{\rho_2^r}{\rho_1^r}\right)^{\gamma_2}$.

4.4. Physical quantities across the right rarefaction wave

Since $\mathbf{\Gamma}_2^3$ is constant in the one-rarefaction wave region, we have

$$u - \int^{\rho_1} \frac{w(\theta)}{\theta} d\theta = u^r - \int^{\rho_1^r} \frac{w(\theta)}{\theta} d\theta,$$

$$u^+ = u^r + f_r(\rho_1^+, V^r), \tag{66}$$

where

$$f_r(\rho_1^+, V^r) = \int_{\rho_1^r}^{\rho_1^+} \frac{w(\theta)}{\theta} d\theta,$$

and

$$\rho_2 = \left(\frac{\rho_2^r}{\rho_1^r}\right)\rho_1. \tag{67}$$

Now, using (67), we obtain for the rarefaction wave an expression of the sum of densities of both the phases as

$$p^+ = g_r = k_1(\rho_1^+)^{\gamma_1} + k_2\left(\frac{\rho_2^r}{\rho_1^r}\right)^{\gamma_2}(\rho_1^+)^{\gamma_2} = k_1(\rho_1^+)^{\gamma_1} + B_2(\rho_1^+)^{\gamma_2}. \tag{68}$$

Thus, the functions f_l and g_l (respectively, f_r and g_r), which govern the relation across the left (respectively, right) and connect the unknown physical quantities to the left (respectively, right) data state V^l (respectively, V^r), have been determined for all the four possible wave patterns. By equating u^- and u^+ from (57) or (59) and (64) or (66), we obtain the following nonlinear equation:

$$f(\rho_1^-, \rho_1^+, V^l, V^r) \equiv f_l + f_r + \Delta u = 0, \tag{69}$$

where $\Delta u = u^r - u^l$, and the functions f_l and f_r are given by

$$f_l(\rho_1^-, V^l) = \begin{cases} \sqrt{A_1(\rho_1^-)^{\gamma_1} + A_2(\rho_1^-)^{\gamma_1-1} + A_3(\rho_1^-)^{\gamma_2} + A_4(\rho_1^-)^{\gamma_2-1} + \dfrac{A_5}{\rho_1^-} + A_6}, & \text{if } \rho_1^l < \rho_1^-, \\ \displaystyle\int_{\rho_1^l}^{\rho_1^-} \frac{w(\theta)}{\theta} d\theta, & \text{if } \rho_1^l \geq \rho_1^-, \end{cases}$$

$$f_r(\rho_1^+, V^r) = \begin{cases} \sqrt{C_1(\rho_1^+)^{\gamma_1} + C_2(\rho_1^+)^{\gamma_1-1} + C_3(\rho_1^+)^{\gamma_2} + C_4(\rho_1^+)^{\gamma_2-1} + \dfrac{C_5}{\rho_1^+} + C_6}, & \text{if } \rho_1^r < \rho_1^+, \\ \displaystyle\int_{\rho_1^r}^{\rho_1^+} \frac{w(\theta)}{\theta} d\theta, & \text{if } \rho_1^r \geq \rho_1^+. \end{cases}$$

By equating p^- and p^+ from (58) or (61) and (65) or (68), we get another algebraic nonlinear equation:

$$g(\rho_1^-, \rho_1^+, V^l, V^r) \equiv g_r(\rho_1^+, V^r) - g_l(\rho_1^-, V^l) = 0, \tag{70}$$

and the functions g_l and g_r are given by

$$g_l(\rho_1^-, V^l) = k_1(\rho_1^-)^{\gamma_1} + B_1(\rho_1^-)^{\gamma_2},$$

$$g_r(\rho_1^+, V^r) = k_1(\rho_1^+)^{\gamma_1} + B_2(\rho_1^+)^{\gamma_2}.$$

5. Numerical algorithm

To validate the proposed Riemann solver of the current paper we solve the model system (12) by using finite volume methods. Such methods solve the Riemann problem (12) with (22) of the current drift-flux model numerically by integrating it over a control volume within the $x - t$ plane

$$\left[x_{i-\frac{1}{2}}, x_{i+\frac{1}{2}}\right] \times [t^n, t^{n+1}], \tag{71}$$

with the dimensions specified by

$$\Delta x = x_{i+\frac{1}{2}} - x_{i-\frac{1}{2}} \quad \text{and} \quad \Delta t = t^{n+1} - t^n, \tag{72}$$

to obtain the following explicit and conservative relation

$$\mathbb{U}_i^{n+1} = \mathbb{U}_i^n - \frac{\Delta t}{\Delta x}\left[\mathbb{F}_{i+\frac{1}{2}} - \mathbb{F}_{i-\frac{1}{2}}\right]. \tag{73}$$

Table 1
Initial data and adiabatic constants for Riemann problem.

Test	ρ_1^l	ρ_2^l	u^l	ρ_1^r	ρ_2^r	u^r	γ_1	γ_2
1	500.0	500.0	32.7169	400.0	400.0	50.0	2.36	1.43
2	1000.0	50.0	−100.0	1000.0	50.0	100.0	2.35	1.43
3	0.9	1.0	0.5	0.9	1.0	−0.5	1.4	1.4
4	901.11	901.11	0.95027	208.88	208.88	0.78548	1.4	1.4

In (73) $\mathbb{U}_i^n$ is the space average approximation within a computational cell of interest at a fixed time t. This is defined as

$$\mathbb{U}_i^n = \frac{1}{\Delta x}\int_{x_{i-\frac{1}{2}}}^{x_{i+\frac{1}{2}}} \mathbb{U}\big(x, t^n\big)dx. \tag{74}$$

Here Δx is the spatial meshing and Δt is the time step that satisfies the known condition

$$\Delta t = \mathrm{CFL}\frac{\Delta x}{S_{\max}^n}, \quad 0 < \mathrm{CFL} \le 1, \tag{75}$$

where CFL is the CourantFriedrichsLewy (CFL) number and $S_{\max}^n$ is the maximum wave speed at time level n chosen as

$$S_{\max}^n = \max_i \big\{|\lambda_i|\big\}, \tag{76}$$

Finally, $\mathbb{F}_{i+\frac{1}{2}}$ is the numerical flux defined at the cell interface $x_{i+\frac{1}{2}}$ as

$$\mathbb{F}_{i+\frac{1}{2}} = \frac{1}{\Delta t}\int_{t^n}^{t^{n+1}} \mathbb{F}\Big(\mathbb{U}\big(x_{i+\frac{1}{2}}, t\big)\Big)dx. \tag{77}$$

The numerical flux can be calculated by using the solution of the local Riemann problem for the current model equations. Such a solution can be analytical or numerical from which a corresponding numerical flux can be used in the context of finite volume methods of interest.

In this work, Godunov methods of centred-type are considered for solving system (12) where the solution of the local Riemann problem is fully numerical. Within this context then we consider two numerical methods, namely, the SLIC scheme and the FORCE scheme. The FORCE scheme is a first-order accurate and stable numerical scheme that approximate the solution to the Riemann problem with initial data $\mathbb{U}^l$ and $\mathbb{U}^r$ by

$$\mathbb{F}_{i+\frac{1}{2}}^{\mathrm{FORCE}}\Big(\mathbb{U}^l, \mathbb{U}^r\Big) = \frac{1}{2}\Big[\mathbb{F}_{i+\frac{1}{2}}^{\mathrm{RI}} + \mathbb{F}_{i+\frac{1}{2}}^{\mathrm{LF}}\Big]. \tag{78}$$

That is, the FORCE scheme is made of the average of the Lax–Friedrichs $\mathbb{F}_{i+\frac{1}{2}}^{\mathrm{LF}}$ and the Richtmyer $\mathbb{F}_{i+\frac{1}{2}}^{\mathrm{RI}}$ fluxes with [29]

$$\mathbb{F}_{i+\frac{1}{2}}^{\mathrm{LF}}\Big(\mathbb{U}^l, \mathbb{U}^r\Big) = \frac{1}{2}\Big[\mathbb{F}(\mathbb{U}^l) + \mathbb{F}(\mathbb{U}^r) + \frac{1}{2}\frac{\Delta x}{\Delta t}[\mathbb{U}^l - \mathbb{U}^r]\Big], \tag{79}$$

and

$$\mathbb{F}_{i+\frac{1}{2}}^{\mathrm{RI}} = \mathbb{F}\Big(\mathbb{U}_{i+\frac{1}{2}}^{\mathrm{RI}}\Big), \tag{80}$$

where

$$\mathbb{U}_{i+\frac{1}{2}}^{\mathrm{RI}}\big(\mathbb{U}^l, \mathbb{U}^r\big) = \frac{1}{2}\big[\mathbb{U}^l + \mathbb{U}^r\big] + \frac{1}{2}\frac{\Delta x}{\Delta t}\big[\mathbb{F}(\mathbb{U}^l) - \mathbb{F}(\mathbb{U}^r)\big]\big].$$

The FORCE scheme is known to have the smallest numerical viscosity and it can be extended to a second-order numerical scheme through the FORCE flux (78). This result in a Total Variation Diminishing (TVD) centred scheme knows as the Slope Limiter Centered (SLIC) scheme which has three steps to employ: data reconstruction, evolution of extrapolated values and the Riemann problem calculation using the FORCE flux (78). The SLIC scheme is well documented in this literature [29,30] and will not be repeated here.

6. Computational results

The proposed exact Riemann solver is assessed through a range of test cases. As mentioned previously, the objective of this paper is to establish a theoretical solution for the Riemann problem of the drift-flux model presented in Section 4. Further, we present comparisons between the exact and numerical solutions in isentropic gas-liquid two-phase flows. This includes a series of test cases. The first test case deals with a pure rarefaction case. In the second test case we consider two rarefaction waves. The third test case is a left shock and right shock waves. In the last test case we present left rarefaction and right shock waves case. Table 1 presents the initial data for all tests in terms of primitive variables. The solution of the Riemann problem with the

Table 2
Solution of the Riemann problem with the initial data from Table 1.

Test	ρ_1^-	ρ_2^-	u^-	ρ_1^+	ρ_2^+
1	400.00739	400.00739	50.00118	400.00739	400.00739
2	492.88627	24.64431	0.0	492.88627	24.64431
3	1.35028	1.50031	0.0	1.35028	1.50031
4	478.88251	478.88251	4.02337	478.88251	478.88251

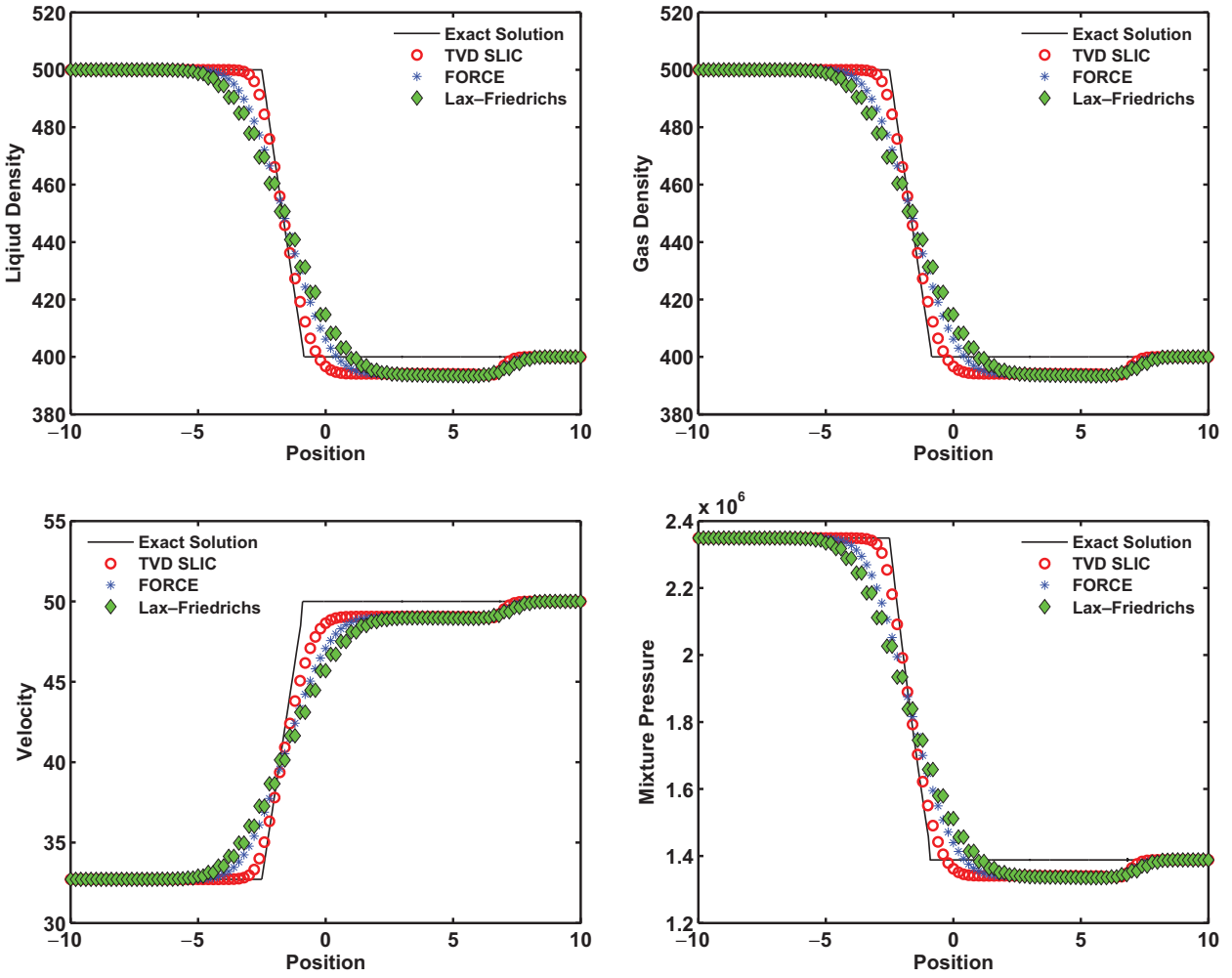

Fig. 1. Pure rarefaction. Solutions for the density of phase 1, phase 2, velocity and pressure at time $t = 0.06$. Exact solutions (solid lines) are compared with three different numerical solutions (symbols): Lax–Friedrichs, FORCE and TVD SLIC. CFL = 0.9 with 100 cells.

given initial data in Table 1 is given in Table 2. From the solution of the Riemann problem of system (12), we illustrate typical wave patterns using MATLAB. In the solution process, we choose to solve the model equations in a one dimensional domain of $[-10, 10]$. Further, transmissive boundary conditions with the SUPERBEE limiter of [29] and with a CFL coefficient of 0.9 are employed for all the numerical methods. Three different numerical methods, namely, the SLIC, FORCE and the Lax–Friedrichs methods are employed to validate the current exact solutions. All numerical results are displayed for such methods on a mesh of 100 cells with appropriate time for each test case. Figs. 1–4 present results for isentropic gas-liquid for $k_1 = 1.0, k_2 = 1.0$ within equations of states given by (7). The symbols in each plot correspond to the numerical solutions approximated by the three different numerical methods. The Lax–Friedrichs scheme shows its known property of paring cell values in all figures as we shall see later. Finally, the solid lines indicate the current exact solutions provided by the exact Riemann solver of the current paper.

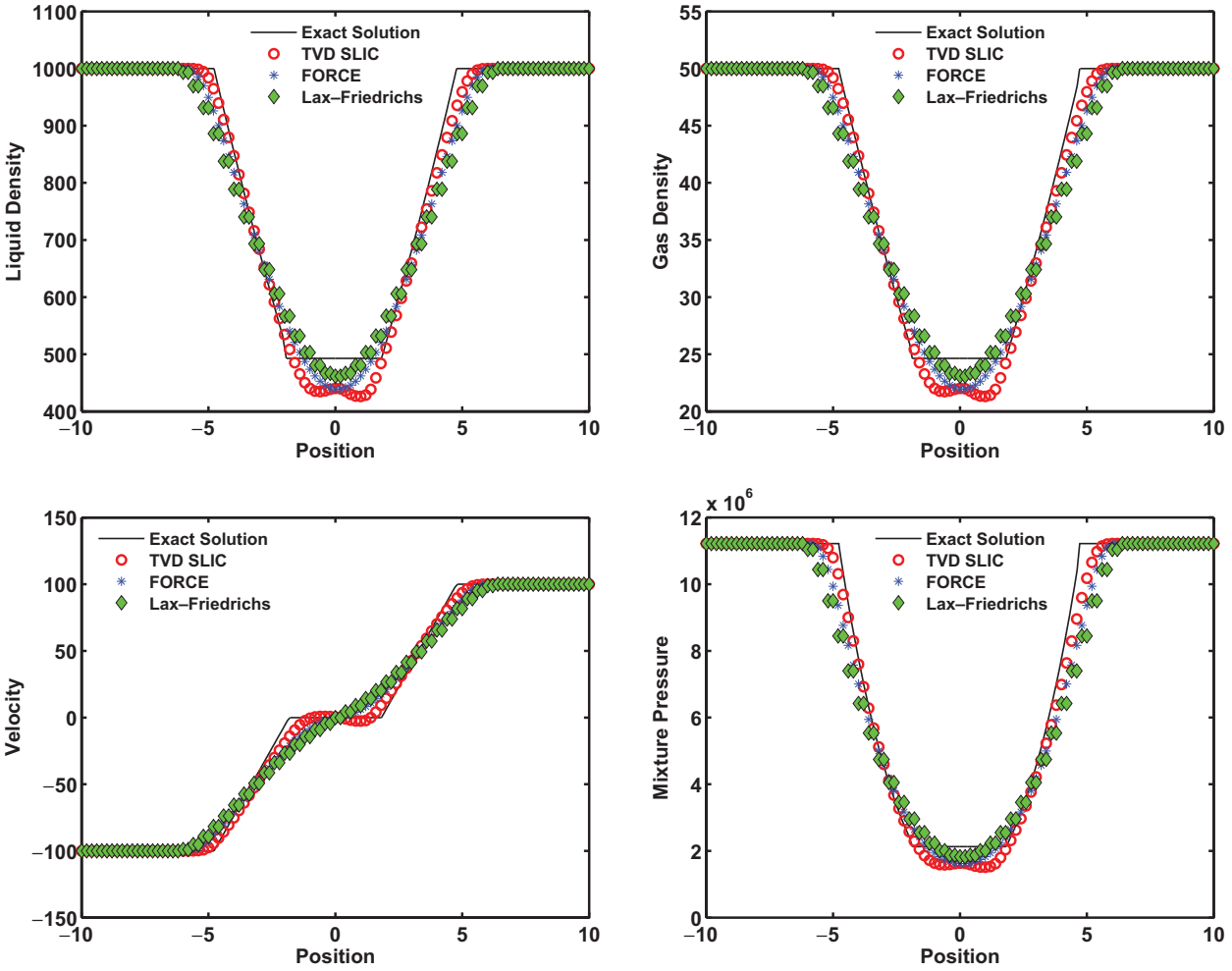

Fig. 2. Rarefaction waves. Analytical and numerical results are compared at $t = 1.85$. The different symbols refer to the Lax–Friedrichs, FORCE and TVD SLIC methods while the solid lines to the exact Riemann solver. CFL = 0.9 with 100 cells for the numerical simulations.

6.1. Pure rarefaction

This test case is the simplest Riemann problem that was originally presented in [31] and investigated in [27,32,33]. Results are displayed in Fig. 1. It consists of a left rarefaction wave only across the complete wave structure. That is, the two-phase flow wave pattern formed by a pure left rarefaction wave associated with the left eigenvalue of the model equations. Fig. 1 presents the exact solution and numerical approximations of the liquid density, gas density, velocity and mixture pressure at time $t = 0.06$. The numerical approximations are calculated with the TVD SLIC, FORCE and Lax–Friedrichs methods on a coarse mesh of 100 cells. The three numerical methods provide the same wave structure as the exact solutions. It is noted that both numerical and exact results are similar to those provided in [27,31–33]. It is also noted that there is a discrepancy or a particular behavior between the exact and numerical results as the wave moving to the right. This is associated to the simplified assumptions within the exact Riemann solution and to the non-linearity of the model equations. Such non-linearity cannot be resolved with current or any other higher order numerical methods on coarse or fine meshes as already observed [27].

6.2. Rarefaction waves

In the second test case, we consider two rarefaction waves and a contact discontinuity. This test case was taken from [34–36] and results are shown in Fig. 2 at time $t = 1.85$. Fig. 2 shows the distributions of liquid density, gas density, velocity and the mixture pressure. The solution contains exact and numerical results. These results are obtained with the developed exact Riemann solver of the current paper, the TVD SLIC, FORCE and Lax–Friedrichs methods. The numerical results provided by the three different numerical methods have apparent discrepancy across the contact discontinuity. However, the numerical results provided by the three different numerical methods are in excellent agreement with the exact solution regardless of such discrepancy. Further,

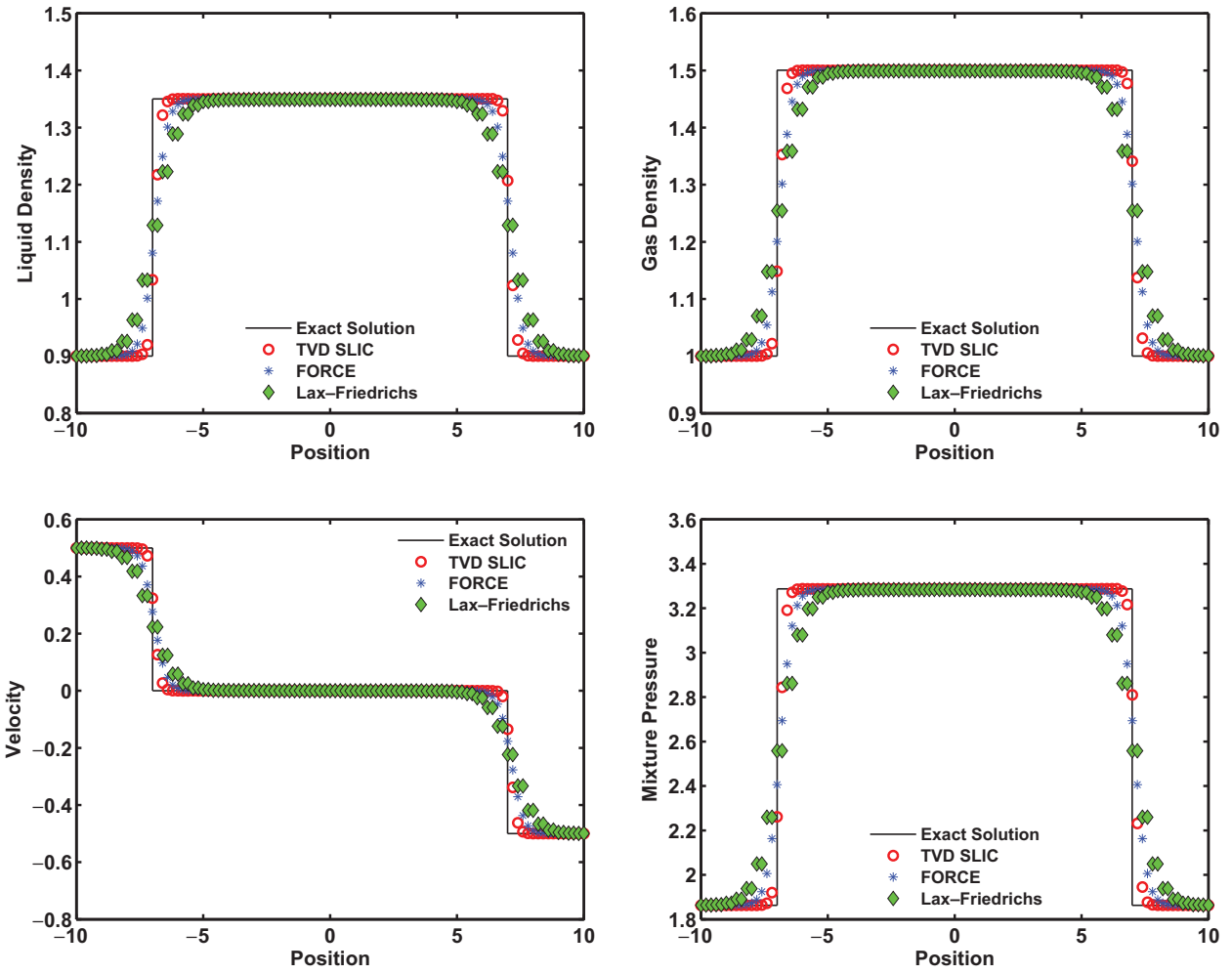

Fig. 3. Shock waves. Left shock and right shock waves test case analytical (solid lines) and numerical (symbols) results are compared at $t = 7.0$. A coarse mesh of 100 cells is used within the Lax–Friedrichs, FORCE and TVD SLIC methods along with the CFL = 0.9.

one can note that both the exact and numerical results predict similar features of the rarefaction waves as proposed originally in [34]. It is also worth to note that both solutions differ in the star region. As has been noticed in the previous test case, this is due to the non-linearity of the model equations as well as the mathematical assumptions of the exact Riemann solver.

6.3. Shock waves

This is a test case from [27]. It consists of shock waves with low phase densities. Solutions are displayed in Fig. 3 at time $t = 7.0$ for the liquid density, gas density, velocity and the mixture pressure. The solid lines represent the results provided by the current exact Riemann solver whereas the symbols refers to the TVD SLIC, FORCE and Lax–Friedrichs methods on a coarse mesh of 100 cells. From the results, it is clear that the present exact Riemann solver are in excellent agreement with those provided using a variety of numerical methods. In comparison with the results of [27], no spurious oscillations are noticeable and the present exact Riemann solver provides similar wave structure. The results presented in Fig. 3 are in agreement with the results of the test case carried out in [27].

6.4. Left rarefaction and right shock waves

The final test case was initially test in [27] which is an extended version of a test case in [31]. The solution of this test case consists of a left rarefaction and right shock waves associated with the left and right eigenvalues λ_1 and λ_3, respectively, and a contact discontinuity associated with λ_2. Results for the liquid density, gas density, velocity and the mixture pressure are presented at time $t = 1.0$ in Fig. 4. In this figure, the exact Riemann solver solutions are compared with three different numerical approximations provided by the TVD SLIC, FORCE and Lax–Friedrichs methods on a coarse mesh of 100 cells. It is noticed that

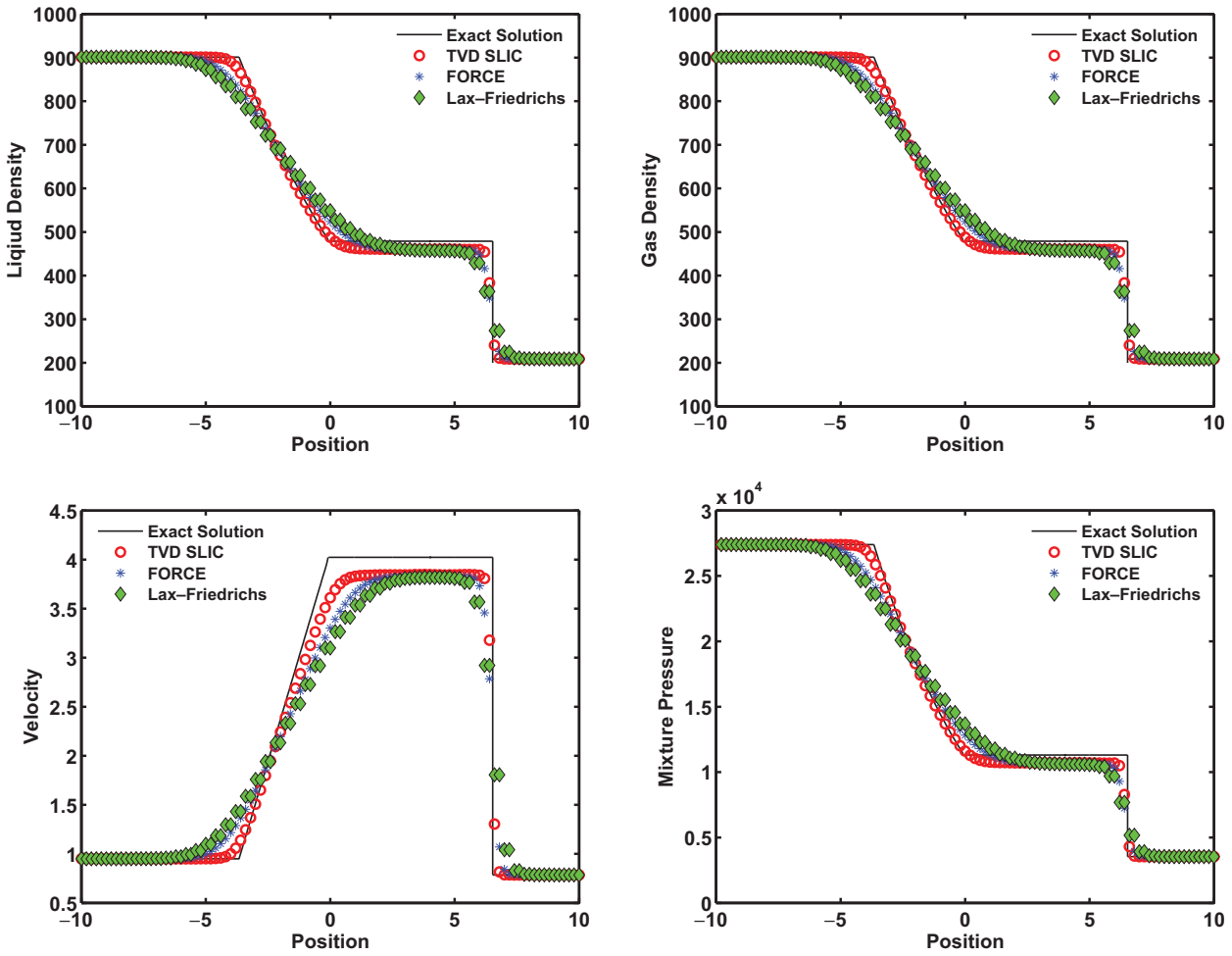

Fig. 4. Left rarefaction and right shock waves. Assessment of exact (solid lines) and numerical solutions (symbols) for the left rarefaction and right shock waves test case at $t = 1.0$. The numerical simulations are provided using the three different numerical methods, namely, the TVD SLIC, FORCE and the Lax–Friedrichs with 100 cells and 0.9 for the CFL stability coefficient.

the three different numerical methods presents excellent agreement with the exact solutions. Particularly, the left rarefaction waves are resolved smoothly as the exact solutions. However, those numerical approximations differ in their ability to resolve the middle wave as it is noted in Fig. 4. That is, the results are slightly different within the star region as one can observe in the velocity plot, see Fig. 4. This is due to the non-linearity of the model equations as noted previously.

With this final test case, it could be concluded that the proposed exact Riemann solver is in good agreement with numerical resolutions that do not require details of the Riemann problem. Solutions also indicate that discrepancies between exact and numerical results occur in all flow variables and are dependent on the initial conditions of the Riemann problem. The Riemann problem for two-phase fluid flow models is an interesting problem which needs to be explored further in the future.

7. Conclusions

This paper presents an exact Riemann solver for a widely used non-linear hyperbolic conservative system of partial differential equations governing the drift-flux model of two-phase flows. Theoretical analysis for the model equations show that all the Riemann waves developed within this paper perform an analytical solution to the Riemann problem. These analyses allowed us to identify several mathematical, physical and numerical properties of the model equations. Based on these analyses and model, we have extended and constructed Godunov methods of centred-type on the basis of finite volume techniques. A key feature of such methods is that the solution of the correspondence Riemann problem is fully numerical. Numerical test cases are presented in the current paper and validate the current theoretical results for the simulation of the drift-flux model. Comparisons between the numerical simulations and theoretical results are matched and in close agreement with analytical solutions for several test cases. It is believed that the proposed solver will be a valid tool to further investigate the drift-flux model mathematically.

In future work, we will present upwind numerical methods based on the developed exact Riemann solver. An important extension is to account for non-isentropic model in one and multiple dimensions. The use of the current exact Riemann solver within the context of complete two-phase flow models is the subject of the next study of the current paper.

Acknowledgments

Research support from National Board for Higher Mathematics, Department of Atomic Energy, Government of India (Ref. no. 2/48(1)/2011/-R&D II/4715) is gratefully acknowledged by first two authors. The third author acknowledges the support as a visiting fellow by the Mathematics Section (Ref. 220(Maths)RR/ab) at the Abdus Salam International Centre for Theoretical Physics (ICTP), Trieste, Italy, 2012.

References

[1] N. Zuber, J.A. Findlay, Average volumetric concentration in two-phase flow systems, J. Heat Transfer Trans. ASME 87 453–469.
[2] M. Ishii, Thermo-fluid Dynamic Theory of Two-Phase Flow, Eyrolles, Paris, 1975.
[3] D.A. Drew, S.L. Passman, Theory of Multicomponent Fluids, Springer, New York, 1999.
[4] H.B. Stewart, B. Wendroff, Two-phase flow: models and methods, J. Comput. Phys. 56 (1984) 363–409.
[5] H. Stadtke, Gas dynamic aspects of two-phase flow: hyperbolicity, wave propagation phenomena, and related numerical methods, Wiley-VCH, Weinheim.
[6] D. Zeidan, Validation of hyperbolic model for two-phase flow in conservative form, Int. J. Comput. Fluid. Dyn. 23 (9) (2009) 623–641.
[7] R. Saurel, R. Abgrall, A multiphase godunov method for compressible multifluid and multiphase flows, J. Comput. Phys. 150 (1999) 425–467.
[8] D. Zeidan, Numerical modelling of the Riemann problem for a mathematical two-phase flow model, in: Computational Methods in Multiphase Flow III, WIT Press, Southampton, 2005, pp. 53–61. WIT Trans Eng Sci 50.
[9] R.I. Issa, M.H.W. Kempf, Simulation of slug flow in horizontal and nearly horizontal pipes with the two-fluid model, Int. J. Multiphase Flow 29 (2003) 69–95.
[10] J.M. Masella, Q.H. Tran, D. Ferre, C. Pauchon, Transient simulation of two-phase flows in pipes, Int. J. Multiphase Flow 24 (1998) 739–755.
[11] A.M. Ansari, N.D. Sylvester, C. Sarica, O. Shoham, J.P. Brill, A comprehensive mechanistic model for upward two-phase flow in wellbores, SPEPF 9 (2) (1994) 143–151.
[12] H. Shi, J.A. Holmes, L.J. Durlofsky, K. Aziz, L.R. Diaz, B. Alkaya, G. Oddie, Drift-flux modeling of two-phase flow in wellbores, SPEJ 10 (1) (2005) 24–33.
[13] A.R. Hasan, C.S. Kabir, Fluid Flow and Heat Transfer in Wellbores, SPE, Richardson, Texas, 2002.
[14] G.B. Wallis, One-Dimensional Two-Phase Flow, McGraw-Hill Book Company, New York, 1969.
[15] A. Hoeld, J.A. Findlay, Coolant channel module CCM: a universally applicable thermalhydraulic drift-flux based mixture-fluid 1d model and code, Nuclear Eng. Des. 237 (2007) 1952–1967.
[16] J.A. Holmes, T. Barkve, O. Lund, Application of a multisegment well model to simulate flow in advanced wells, spe paper 50646, presented at the European Petroleum Conference (1998). The Hague, Netherlands, Oct 20-22.
[17] H. Cao, Development of techniques for general purpose simulators, 2002 (Ph.D. thesis). Ph.D. dissertation, Stanford University.
[18] G.P. Nassos, S.G. Bankoff, Slip velocity ratios in an air-water system under steady-state and transient conditions, Chem. Eng. Sci. 22 (4) (1967) 661–668.
[19] L. Pan, S.W. Webb, C.M. Oldenburg, Analytical solution for two-phase flow in a wellbore using the drift-flux model, I. J. Adv. Water Resour. 34 (2011) 1656–1665.
[20] L. Pan, C.M. Oldenburg, K.P. Y. S. Wu, T2well/eco2n version 1.0: multiphase and non-isothermal model for coupled wellbore-reservoir flow of carbon dioxide and water, LBNL-4291E (2010).
[21] L. Pan, C.M. Oldenburg, Y.S. Wu, K. Pruess, Wellbore flow model for carbon dioxide and brine, Energy Proc. 1 (1) (2009). 71-8. Proceedings of GHGT9 (2008) Washington DC LBNL-1416E, November 16–20, 2008.
[22] K. Pruess, C.M. Oldenburg, G.J. Moridis, Tough2 users guide version 2, E O Lawrence Berkeley National Laboratory Report LBNL-43134, 1999.
[23] N. Andrianov, G. Warnecke, The Riemann problem for the Baer-Nunziato two-phase flow model, J. Comput. Phys. 195 (2004) 434–464.
[24] M.R. Baer, J.W. Nunziato, A two-phase mixture theory for the deflagration-to-detonation transition (ddt) in reactive granular materials, Int. J. Multiphase Flows 12 (1986) 861–889.
[25] D.W. Schwendeman, C.W. Wahle, A.K. Kapila, The Riemann problem and a high-resolution godunov method for a model of compressible two-phase flow, J. Comput. Phys. 212 (2) (2006) 490–526.
[26] C.E. Castro, E.F. Toro, A Riemann solver and upwind methods for a two-phase flow model in nonconservative form, Int. J. Numerical Methods Fluids 50 (2006) 275–307.
[27] D. Zeidan, The Riemann problem for a hyperbolic model of two-phase flow in conservative form, Int. J. Comput. Fluid. Dyn. 25 (6) (2011) 299–318.
[28] M.K. Banda, M. Herty, J.T. Ngnotchouye, Toward a mathematical analysis for drift-flux multiphase flow models in networks, SIAM J. Sci. Comput. 31 (6) (2010) 4633–4653.
[29] E.F. Toro, Riemann Solvers and Numerical Methods for Fluid Dynamics, Springer-Verlag, Berlin, 2009.
[30] D. Zeidan, Numerical resolution for a compressible two-phase flow model based on the theory of thermodynamically compatible systems, Appl. Math. Comput. 217 (11) (2011) 5023–5040.
[31] M. Baudin, et al., A relaxation method for two-phase flow models with hydrodynamic closure law., Numerische Mathematik 99 (2005) 411–440.
[32] M. Baudin, et al., A semi-implicit relaxation scheme for modeling two-phase flow in a pipeline, SIAM J. Sci. Comput. 27 (2005) 914–936.
[33] S.T. Munkejord, et al., The multi-stage centred-scheme approach applied to a drift-flux two-phase flow model, Int. J. Numerical Methods Fluids 52 (2006) 679–705.
[34] R. Saurel, et al., Simple and efficient relaxation methods for interfaces separating compressible fluids, cavitating flows and shocks in multiphase mixtures, J. Comput. Phys. 228 (2009) 1678–1712.
[35] E. Goncalvès, Numerical study of expansion tube problems, Comput. Fluids 72 (2013) 1–19.
[36] D. Zeidan, E. Goncalvès, A. Slaouti, Computer simulations of cavitating two-phase flows, AIP Conf. Proc. 1558 (2013) 208–211.